forests

Article

Forest Height Inversion via RVoG Model and Its Uncertainties Analysis via Bayesian Framework—Comparisons of Different Wavelengths and Baselines

Yongxin Zhang [1], Han Zhao [1], Yongjie Ji [2,*], Tingwei Zhang [1] and Wangfei Zhang [1]

1 College of Forestry, Southwest Forestry University, Kunming 650224, China
2 School of Geography and Ecotourism, Southwest Forestry University, Kunming 650224, China
* Correspondence: jiyongjie@live.cn

Abstract: Accurate estimation of forest height over a large area is beneficial to reduce the uncertainty of forest carbon sink estimation, which is of great significance to the terrestrial carbon cycle, global climate change, forest resource management, and forest-related scientific research. Forest height inversion using polarimetric interferometry synthetic aperture radar (PolInSAR) data through Random volume over ground (RVoG) models has demonstrated great potential for large-area forest height mapping. However, the wavelength and baseline length used for the PolInSAR data acquisition plays an important role during the forest height estimation procedure. In this paper, X–, C–, L–, and P–band PolInSAR datasets with four different baseline lengths were simulated and applied to explore the effects of wavelength and baseline length on forest height inversion using RVoG models. Hierarchical Bayesian models developed with a likelihood function of RVoG model were developed for estimated results uncertainty quantification and decrease. Then a similar procedure was applied in the L– and P–band airborne PolInSAR datasets with three different baselines for each band. The results showed that (1) Wavelength showed obvious effects on forest height inversion results with the RVoG model. For the simulated PolInSAR datasets, the L– and P–bands performed better than the X– and C–bands. The best performance was obtained at the P–band with a baseline combination of 10 × 4 m with an absolute error of 0.05 m and an accuracy of 97%. For the airborne PolInSAR datasets, an L–band with the longest baseline of 24 m in this study showed the best performance with R^2 = 0.64, RMSE = 3.32 m, and Acc. = 77.78%. (2) It is crucial to select suitable baseline lengths to obtain accurate forest height estimation results. In the four baseline combinations of simulated PolInSAR datasets, the baseline combination of 10 × 4 m both at the L– and P–bands performed best than other baseline combinations. While for the airborne PolInSAR datasets, the longest baseline in three different baselines obtained the highest accuracy at both L– and P–bands. (3) Bayesian framework is useful for estimation results uncertainty quantification and decrease. The uncertainties related to wavelength and baseline length. The uncertainties were reduced obviously at longer wavelengths and suitable baselines.

Keywords: PolInSAR; forest height; RvoG model; baseline length; wavelength; uncertainties

check for updates

Citation: Zhang, Y.; Zhao, H.; Ji, Y.; Zhang, T.; Zhang, W. Forest Height Inversion via RVoG Model and Its Uncertainties Analysis via Bayesian Framework—Comparisons of Different Wavelengths and Baselines. *Forests* **2023**, *14*, 1408. https://doi.org/10.3390/f14071408

Academic Editor: Gherardo Chirici

Received: 13 May 2023
Revised: 27 June 2023
Accepted: 8 July 2023
Published: 10 July 2023

1. Introduction

Forests are natural resources and carbon reservoirs. Humans depend on them for survival since the air we breathe and the wood we use are partly coming from forests. In addition to providing habitat for animals and livelihoods for humans, forests play an important role in global ecosystem security by preventing soil erosion and mitigating climate change through interactions with the atmosphere and soil [1–4]. As an important forest parameter, the accurate estimation of forest height can provide information on forest health, and the forest height is also an important indicator for estimating the productivity of forest wood volume. In addition, forest height is often used as an input variable in biomass estimation models because of its close association with forest Above Ground Biomass (AGB) and carbon stock [5,6].

The estimation methods for stand height obtained at regional or global scales, also known as stand mean height or forest height, rely on remote sensing techniques, the sensitivity of remote sensing data sources to forest vertical structure, and meteorology, limiting the accuracy and continuity of their estimation [7]. Synthetic Aperture Radar (SAR) signals have a certain penetration capability into the forest and can interact with the organs of the forest tree deeply in the vegetation layer to provide better information on the vertical vegetation profile, and thus are a powerful tool for extracting the vertical structure parameters of the forest. Moreover, SAR data overcoming both the weather and time-dependent factors of optical data has great potential for regional and global largescale forest height inversion [8,9]. With the development of SAR imaging technology, the methods for forest structure information identification based on SAR technology gradually tend to diversify, gradually developing from the initial single-polarization, single-band and single-baseline to the current multi-polarization, multi-band and multi-baseline and other different observation methods and their combinations. Among them, Polarimetric Synthetic Aperture Radar (PolSAR) has been widely used in surface classification because it can reflect the properties of scatterers since different scattering mechanisms can be reflected by different polarization information [10–12]. Interferometric Synthetic Aperture Radar (InSAR) can reflect the elevation information of scattering objects through phase difference to obtain more accurate elevation measurement results, and InSAR has become a powerful tool for many applications [13]. Polarimetric Synthetic Aperture Radar Interferometry (PolInSAR), which has the advantages of both PolSAR and InSAR, has become a powerful tool for vegetation height inversion, Digital Elevation Model (DEM) generation, feature classification, and area change detection studies [14–16].

There are three main ways to perform the inversion of tree height using PolInSAR. The first way considers the phase center of HV polarization corresponding to the scattering phase center of the forest canopy and the phase center of HH–VV polarization corresponding to the surface scattering phase center and uses the difference between the above two phase centers to obtain the forest height [17]. However, the above method results in the underestimation of forest height due to the fact that in some bands, the phase centers of HV and HH–VV polarization are not significantly different [18]. The second way is to construct the scattering vector complex coherence, i.e., first calculating the complex coherence representing the canopy scattering mechanism and the forest surface scattering; both of them are then separated by a coherence optimization algorithm (e.g., PD polarization coherence optimization algorithm). Next, the phase difference between the two optimized phase center difference is used to estimate the forest height. The third way is to establish a forest microwave scattering model, through which the link between the interference coherence, the interference phase, and the forest height is established, and then the forest height is inversed through the constructed models. Currently, RVoG (Random Vegetation over Ground) model, which assumes the forest as a two−layer model, is widely applied for forest height inversion [19–22]. In order to estimate forest height, many algorithms based on the RVoG model have been proposed. Cloude and Papathanassiou combined the polarized interferometric coherent optimization algorithm with the RVoG model and proposed to invert the mean vegetation height and extinction coefficient by using a least squares model of the vegetation parameters, but this method requires a nonlinear iterative algorithm to invert the six-dimensional parameters, which is more complex and strictly depends on the initial value setting [17]. However, in order to avoid the rank deficiency problem in the above six-dimensional nonlinear optimization processing, Cloude et al. (2003) proposed a three-stage algorithm [17]. This algorithm considers the geometric representation of RVoG in a complex unit circle (CUC) and uses a least-square line fit to estimate the ground phase. To further reduce the number of unknown parameters, the ground-volume scattering ratio can be assumed to be 0, and a two-dimensional look-up table is used to calculate the forest height and extinction coefficient. Dubois–Fernandez et al. (2008) and Garestier et al. (2008) proposed an improved three-phase algorithm based on long wavelength SAR, fixed to the extinction coefficient instead of the ground-volume scattering ratio [23,24]. Compared with the six-dimensional nonlinear iterative algorithm, the two three-stage algorithms take into account the geometric properties of the RVoG model to improve reliability and practicability. In addition, Zhu et al. (2014) extended the least-squares adjustment from the real domain to the complex domain and proposed a complex least-squares algorithm and obtained more accurate forest height results [25].

In addition to forest height inversion using RVoG models, the inversion uncertainties resulting from RVoG model parameters and observations were explored in recent decades. Riel et al. (2018) addressed the errors in the PolInSAR data and the errors due to incorrect RVoG modeling assumptions and proposed a Bayesian framework that can be used to estimate the uncertainties resulting from the RVoG model parameters for a given PolInSAR complex coherence [26]. Kugler et al. (2014) investigated the effects of vertical wavenumber (k_z) on the performance of forest height estimation. The results demonstrated that a single k_z only provides accurate inversion of forest height over a limited range, and multiple PolInSAR acquisitions with variables are required to obtain accurate inversions over a large range [27,28].

Although the above-mentioned exploring of forest height inversion and the uncertainties using PolInSAR data and RvoG models, there are still scientific gaps in forest height inversion using RvoG models, and the uncertainties in the estimated results from different sources need to be further explored in detail. In this paper, four widely used forest height inversion microwave bands, including X–, C–, L–, and P–band with four baseline sets, were simulated and applied for forest height inversion, and their uncertainties resulted from different sources analysis. The RVoG model and Bayesian frameworks were applied for forest height inversion and uncertainties quantification, respectively. The procedures were applied in the L– and P–band airborne PolInSAR data with three baseline sets to make sure the uncertainties resulted from different wavelengths and baselines.

2. Background

2.1. PolInSAR Principles

Conventional interferometry usually uses single-polarization data, while polarized interferometry uses fully polarized data, which is represented as a scattering matrix, so the scattering matrix needs to be vectorized first. Since the vectorization using the Pauli orthogonal is easier to interpret the scattering mechanism, therefore, the scattering matrix is generally vectorized using the Pauli basis as follows:

$$\bar{k} = \frac{1}{2}Trace\big([S]\psi_p\big) = \frac{1}{\sqrt{2}}\{s_{\mathrm{hh}} + s_{\mathrm{vv}}, s_{\mathrm{hh}} - s_{\mathrm{vv}}, s_{\mathrm{hv}} + s_{\mathrm{vh}}, i(s_{\mathrm{hv}} - s_{\mathrm{vh}})\} \tag{1}$$

Under the condition that the scatterers satisfy the reciprocity, i.e., $s_{\mathrm{hv}} = s_{\mathrm{vh}}$, the coherent scattering vector can be simplified as:

$$\bar{k} = \frac{1}{\sqrt{2}}\{s_{\mathrm{hh}} + s_{\mathrm{vv}}, s_{\mathrm{hh}} - s_{\mathrm{vv}}, 2s_{\mathrm{hv}}\} \tag{2}$$

The primary and secondary images are vectorized as k_1 and k_2, and their conjugates are multiplied to obtain the T_6 matrix:

$$T_6 = \begin{bmatrix} k_1 \\ k_2 \end{bmatrix}\left[k_1^{*T} {k_2}^{*T}\right] = \begin{bmatrix} T_{11} & \Omega_{12} \\ {\Omega_{12}}^{*T} & T_{22} \end{bmatrix} \tag{3}$$

where $[T_{11}]$ and $[T_{22}]$ are the standard Ermitian correlation matrices, they contain the polarization information of the primary and secondary images, and $[\Omega_{12}]$ contains not only the polarization information but also the interference information between the primary and secondary images.

In order to be able to obtain all the information in the scattering space from fully polarized data, it is necessary to define two unit vectors w_1 and w_2 representing specific scattering mechanisms and project the scattering vectors k_1 and k_2 onto w_1 and w_2 to obtain the information of the feature on the scattering mechanisms w_1 and w_2, corresponding to images i_1 and i_2.

$$\begin{array}{c} i_1 = w_1^{*T} \cdot k_1 \\ i_2 = w_{1}{}_2^{*T} \cdot k_2 \end{array} \tag{4}$$

By multiplying i_1 and i_2 conjugately, we obtain the interference information $i_1 i_2^*$ of the feature under the specific scattering mechanisms w_1 and w_2

$$i_1 i_2^* = \left(w_1^{*T} \cdot k_1\right)\left(w_2^{*T} \cdot k_2\right)^* = w_1^{*T}\left(k_1 \cdot k_2^{*T}\right) w_2 = w_1^{*T} \Omega_{12} w_2 \tag{5}$$

The interferometric complex coherence of the two images can be expressed as:

$$\widetilde{\gamma}(w_1, w_2) = \frac{w_1^{*T} \Omega_{12} w_2}{\sqrt{w_1^{*T} T_{11} w_1 \cdot w_2^{*T} T_{22} w_2}} \tag{6}$$

2.2. RVoG Model

Similar to the traditional quantitative inversion of remote sensing, forest height is not directly observed by SAR data, and a vegetation scattering model is needed to connect SAR parameters with the scattering process of the features. Several vegetation coherent scattering models have been proposed for forest applications, mainly including the Interferometric Water Cloud Model (IWCM) [29,30], the Two−level Method (TLM) [31], and the RVoG model [19]. The RVoG model was proposed by Treuhaft in 1996 and is widely used in forest height inversions due to its simplicity and high accuracy [19].

The RVoG model assumes a two−layer structure, where the upper scattering layer represents forest canopy scattering and the lower scattering layer represents surface scattering. The classical form of the RVoG model can be expressed as Equation (7) [18,26,32,33].

$$\widetilde{\gamma}(\underline{w}) = e^{i\phi} \frac{\widetilde{\gamma}_v + \mu(\underline{w})}{1 + \mu(\underline{w})} = e^{i\phi}\left[\widetilde{\gamma}_v + \frac{\mu(\underline{w})}{1 + \mu(\underline{w})}(1 - \widetilde{\gamma}_v)\right] \tag{7}$$

where $e^{i\phi} = \mathrm{k}_z z_0$ denotes the ground phase, $\mu(\underline{w})$ denotes the ground body scattering ratio, and $\widetilde{\gamma}_v$ denotes the coherence caused by scattering from vegetative bodies only, which can be expressed as:

$$\gamma_v = \frac{I_2}{I_1} = \frac{\int_0^h f(z) \mathrm{e}^{\mathrm{j}k_c z} \mathrm{d}z}{\int_0^{h_2} \mathrm{f}(z) \mathrm{d}z} = \frac{2\sigma}{\cos\left(\mathrm{e}^{2\sigma b_2 / \cos(0)} - 1\right)} \int_0^1 \mathrm{e}^{ik_z} \mathrm{e} \, \mathrm{e}^{\frac{2\sigma z}{\cos s}} \mathrm{d}z = \frac{p}{p_1} \frac{e^{p_1 h_v} - 1}{e^{p h_v} - 1} \tag{8}$$

$$\begin{cases} p = \frac{2\sigma}{\cos\theta} \\ p_1 = p + ik_z \\ k_z = \frac{4\pi\Delta\theta}{\lambda \sin\theta} \approx \frac{4\pi B_n}{\lambda H \tan\theta} \end{cases} \tag{9}$$

where σ is the average extinction coefficient, θ is the incidence angle, $\Delta\theta$ is the incidence angle difference caused by the baseline, H is the sensor flight altitude, B_n is the vertical baseline, and λ is the wavelength of the electromagnetic wave.

2.3. Bayesian Statistical Model

2.3.1. Bayesian Model

Bayesian methods begin by specifying a prior distribution of the parameters that must be estimated. The prior reflects the information known to the researcher without reference to the dataset from which the model is estimated. In the case of time series, the prior can be formed by looking at out-of-sample historical data. Denote by θ the parameters to be estimated and by $p(\theta)$ the prior beliefs about these parameters. If the observed sample is y, the posterior density of θ for a given sample can be written as:

$$p(\theta \mid y) \propto p(\mathrm{y} \mid \theta) p(\theta) \tag{10}$$

$p(\theta)$ is the prior distribution, which reflects our knowledge and understanding of the parameters to be estimated before the data are observed; $p(\mathrm{y} \mid \theta)$ is the likelihood function, which is a description of the actual observed data; and $p(\theta \mid y)$ is the posterior distribution, which is the final analysis result obtained by Bayes' theorem.

2.3.2. Multi-Parameter Bayesian Model

The multi-parameter Bayesian model is more than one input parameter, and the multi-parameter form of the Bayesian model is given in Equation (11)

$$p(\theta_1, \ldots, \theta_2 \mid y) \propto p(\mathrm{y} \mid \theta_1, \ldots, \theta_2) p(\theta_1, \ldots, \theta_2) \tag{11}$$

Hierarchical Bayesian models are constructed by using a hyper-prior on top of the prior. By adding the hyper-prior, the new model has an additional layer compared to the original model to reflect the multiple sources of uncertainty in the modeling process, such as uncertainty caused by model input parameters, model theoretical assumptions, observations, etc. Moreover, by building a layered model, over-fitting problems caused by too many model parameters can also be avoided. Overfitting problems caused by too many model parameters can also be avoided by building hierarchical models [17].

2.3.3. A Hierarchical Bayesian Framework Based on the RVoG Model

By using the Bayesian framework, we can relate the probability of any prior information that we have about the canopy parameters in the RVoG model, the error model that we expect for the observations, and the distribution of predicted values of the canopy parameters that we expect for the observations with a hierarchical Bayesian framework The Bayesian framework based on the RVoG model can be expressed by the Equation below.

$$p(\mathrm{m} \mid \gamma, \mathcal{R}(\mathrm{m})) \propto p(\gamma \mid \mathrm{m}, \mathcal{R}(\mathrm{m}), \sigma_\gamma) p(\mathrm{m}) \tag{12}$$

where the posterior distribution $p(\mathrm{m} \mid \gamma, \mathcal{R}(\mathrm{m}))$ of the canopy parameters is proportional to the likelihood function $p(\gamma \mid \mathrm{m}, \mathcal{R}(\mathrm{m}), \sigma_\gamma)$ of the data and the prior distribution $p(\mathrm{m})$.The flexibility of the Bayesian model allows us to use more complex error models. That is, adding the hyper-prior $p(\sigma_\gamma)$ to Equation (13) makes it a hierarchical Bayesian model.

$$p(\mathrm{m}, \sigma_\gamma \mid \gamma, \mathcal{R}(\mathrm{m})) \propto p(\gamma \mid \mathrm{m}, \mathcal{R}(\mathrm{m}), \sigma_\gamma) p(\mathrm{m}) p(\sigma_\gamma) \tag{13}$$

The super prior $p(\sigma_\gamma)$ is the variance σ_γ of the a priori distribution to redefine the uncertainty (mean known, variance unknown variance) of the distribution. In this way, the observation error and uncertainty due to model assumptions can be expressed in this way as the random σ_γ. The posterior distribution $p(\mathrm{m}, \sigma_\gamma \mid \gamma, \mathcal{R}(\mathrm{m}))$ is the joint distribution by which we obtain the sampling chain of the posterior distribution of forest height of h_v and uncertainties of σ_γ [34].

More information on the uncertainty analysis of the RVoG model based on the Bayesian framework, readers are referred to in [26].

2.4. Metropolis–Hastings Algorithm

Although the posterior distribution of the parameters can be obtained using the Bayesian framework, most models have difficulty in obtaining a closed analytic posterior distribution function and therefore require numerical methods to compute the posterior. When the analytic posterior is not available, the Markov Chain Monte Carlo (MCMC) method was used for random sampling according to the posterior distribution [35,36]. The Metropolis–Hastings algorithm is the most commonly used MCMC algorithm. The iterative steps of the Metropolis–Hastings algorithm in this study include five main steps as follows:

(1) Give the parameters an initial state based on random initialization or empirical values, i.e., initialize the initial state of the Markov chain;

(2) Generate a new state from some distribution for model likelihood function—here for RVoG model parameters is Gaussian distribution—for model estimation errors as an inverse gamma hyperprior function;
(3) Calculate the probability of accepting the new parameter according to the Metropolis–Hastings criterion. Here, the acceptance rules are the same as [26];
(4) A random sample of data points from the interval [0, 1] (uniform distribution). $u \sim U[0,1]$. The randomly generated number is compared with the acceptance rate, and if the value of the number is less than the probability calculated in step (3), then the new state is accepted. Otherwise, it continues to remain in the original state.
(5) Go back to step (2) and iterate again until enough samples are generated.

2.5. Uncertainty Evaluation Indicators

In this study, Absolute error (δ, Equation (14)), Predictive accuracy (*Acc*, Equation (15)), and Standard deviation (Sd) ($S_{\overline{X}}$, Equation (16)) are used to quantify the uncertainty of the inversed results [37,38].

$$\delta = x - \mu \tag{14}$$

$$Acc. = \left(1 - \frac{|\delta|}{x}\right) \tag{15}$$

$$S_{\overline{X}} = \sqrt{\frac{\sum_{i=1}^{n}\left(X_i - \overline{X}\right)^2}{n(n-1)}} \tag{16}$$

where x is true value, μ is predicted value, δ is absolute error, X_i is the sample of forest height inversion results obtained from PolInSAR data, n is the number of elements contained in the observation sample, $\overline{X}$ is the arithmetic mean of each observation, and $S_{\overline{X}}$ is the standard error.

3. Methods

3.1. Simulated Data

The simulated PolInSAR datasets are generated by the PolSARProSIM module in PolSARPro software developed by European Space Agency (ESA), which has a similar operation to an airborne platform and ignores residual motion, baseline, and alignment errors, as well as the time and signal-to-noise de-correlation effects [39]. In this study, 16 PolInSAR datasets at four bands, like the X–, C–, L–, and P–band, were generated, with four different baselines at each band. The simulated data image sizes were all 141 × 105 pixels, the true forest height was set as 18 m, the forest density was 300 plants/ha, the platform heights were all 3000 m, the central incidence angle was 45°, and the forest structure was all broadleaf trees. The detailed information of the simulated 16 PolInSAR datasets is summarized in Table 1.

Table 1. The parameters of 16 simulated PolInSAR datasets.

Band	Center Frequency	Azimuthal Resolution	Range Resolution	Horizontal Baseline	Vertical Baseline
X–	9.6/GHz	1.5 m	1.06 m	10 m	2 m 4 m 6 m 8 m
C–	5.35/GHz	1.5 m	1.06 m	10 m	2 m 4 m 6 m 8 m

Table 1. *Cont.*

Band	Center Frequency	Azimuthal Resolution	Range Resolution	Horizontal Baseline	Vertical Baseline
L–	1.3/GHz	1.5 m	1.06 m	10 m	2 m 4 m 6 m 8 m
P–	0.65/GHz	1.5 m	1.06 m	10 m	2 m 4 m 6 m 8 m

The simulated forest scenes for the four bands used in this study are shown in Figure 1. The simulated forests are broadleaf forests located on flat ground (10 m horizontal baseline and 8 m vertical baseline as an example), the mean forest height is set as 18 m and forest density to 300 plants/hm^2, and the soil moisture content and soil roughness in these scenes are set as 0.

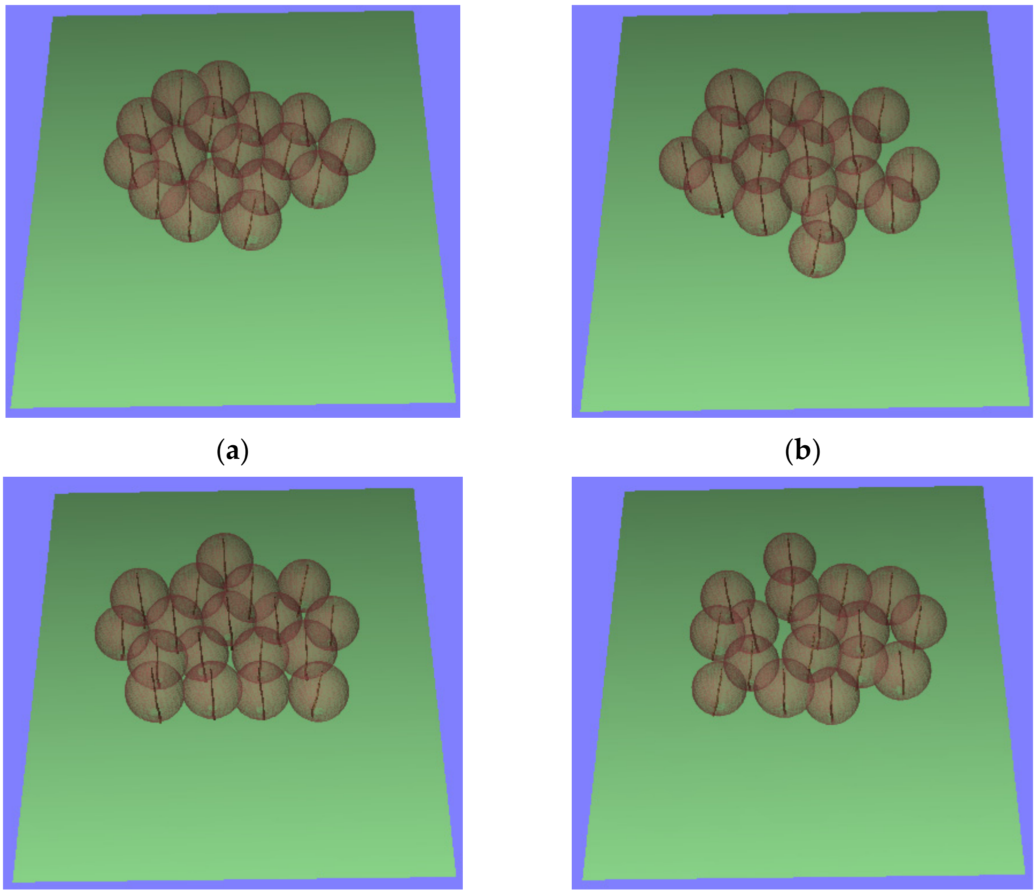

(**a**) (**b**)

(**c**) (**d**)

Figure 1. Forest scene of broadleaf forest. (**a**) X–band; (**b**) C–band; (**c**) L–band; (**d**) P–band.

For the simulated PolInSAR datasets, we first use the master and slave images to generate the interferogram as in Figure 2a, from which we can see the obvious flatland effect. And the forest height inversion is seriously affected by the flat earth effect, so it needs to remove the flat earth effect, which is shown in Figure 2b. The interferometric phase with the removed flat earth effect is shown in Figure 2c. Then, a 7 × 7 window is used for the complex coherence estimation.

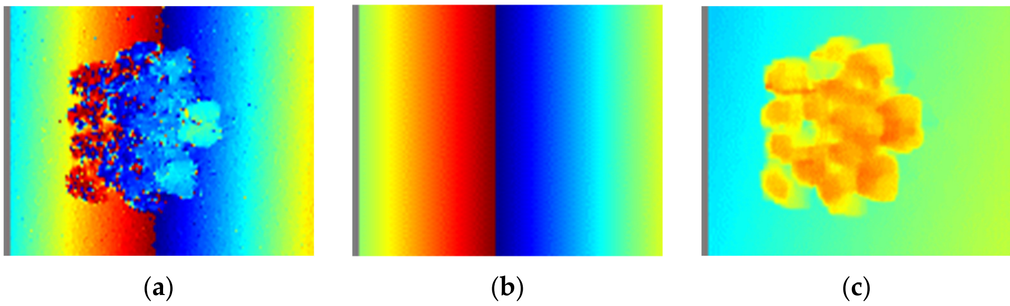

Figure 2. Interference phase (L–band). (**a**) Interferogram before de–flattening; (**b**) Flat Earth Phase; (**c**) Interferogram after de–flattening.

According to Equation (9), we know that the spatial baseline length is related to the vertical effective wave number k_z, then the relationship between them is briefly addressed here. k_z is a key parameter in the RVoG model, which reflects the sensitivity of the height to interferometric observations and is crucial to the inversion of forest height. The effect of k_z on the forest height inversion is that when the forest height is fixed, during a range of k_z, the larger k_z is, the more serious the decoherence caused by the scattering of vegetation; when k_z fixed, in a range of forest height, the higher the forest height, the more the volume scattering decoherence [6]. Moreover, the relationship is affected by forest structure through different extinction values. In this study, the extinction value is fixed at each band according to previous studies. Figure 3 shows the histograms of k_z values of the simulated data at each band with different baselines.

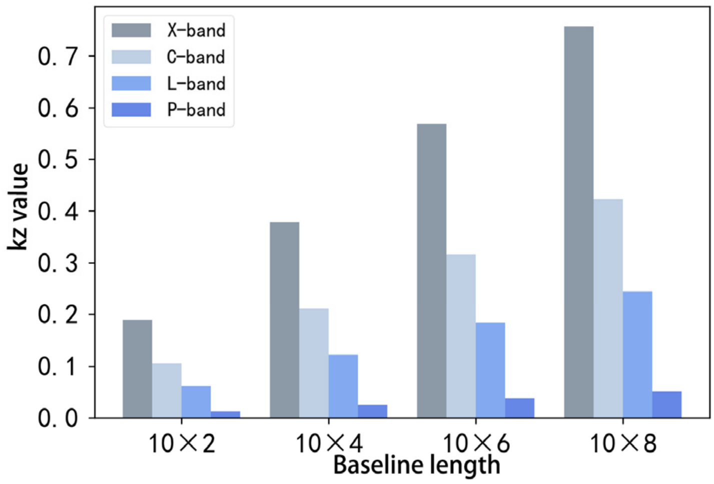

Figure 3. k_z of each band at different baselines.

3.2. Airborne PolInSAR Data

3.2.1. Data Profile

The airborne PolInSAR data used in this study were collected by DLR (German Aerospace Center) and Swedish Defence Research Agency (FOI) using an airborne ESAR system in the Krycklan region of Sweden in October 2008 in BioSAR2008 projects. Three L–band PolInSAR aerial flight datasets and three P–band PolInSAR aerial flight datasets were selected in this study. The data incidence angles of the two bands vary from about 25° to 55°, where the P–band data have an azimuthal sampling of 0.74 m and a range sampling of 1.50 m, and the L–band data have an azimuthal sampling of 0.47 m and a range sampling of 1.50 m. The coverage of the L– and P–band SAR datasets is shown in Figure 4. All the datasets were acquired in full polarization mode. Detailed information about the imaging configuration parameters is shown in Table 2.

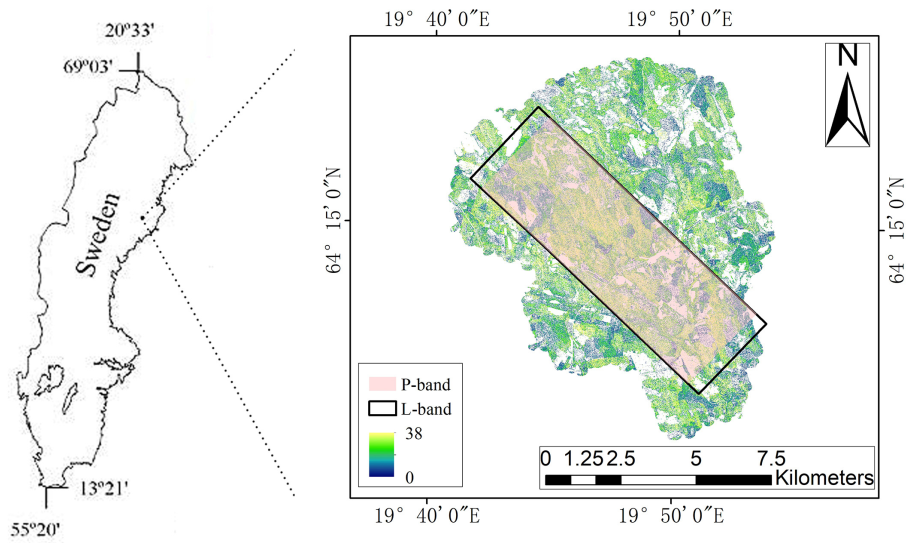

Figure 4. Location of the study area in Sweden.

Table 2. Different PolInSAR interference image parameters.

Master	Slave	Band	Spatial Baseline [m]	k_z [rad/m]	No.
BioSAR201	BioSAR203	L	6	0.0652	B1
BioSAR201	BioSAR205	L	12	0.1369	B2
BioSAR201	BioSAR207	L	18	0.2007	B3
BioSAR103	BioSAR105	P	8	0.0278	B4
BioSAR103	BioSAR107	P	16	0.0555	B5
BioSAR103	BioSAR109	P	24	0.0793	B6

LiDAR data was also obtained Through the BioSAR2008 project. The resolution of LiDAR–derived products is 0.5 m × 0.5 m. The coverage of the LiDAR data is shown in Figure 4.

3.2.2. Study Area

The study area is located in a forested area in northern Sweden (64°14′ N, 19°46′ E), with a basin area of about 6700 hm^2. The overall topography in the study area is flat, with a maximum slope of 20° and an elevation ranging from 100 m to 400 m. The study area is rich in forest resources, the vegetation type of the region in the northern hemisphere is cold-temperate vegetation, and the forest types are mainly coniferous and broad-leaved forests, among which the dominant species of coniferous forests are Scots pine (*Pinus sylvestris*) and Norway spruce (*Picea abies*), the dominant species of broad-leaved forests are birch (*Betula* spp.) [40].

3.2.3. PolInSRA Data Pre-Processing

Since the data of BioSAR2008 acquired in this study has been accurately co-registered, it can be used directly for obtaining interferometric phase and coherence. Before the complex coherence estimation, the phase differences caused by the flat earth were removed. Then, an 11 × 11 window is used for complex coherence calculation. The obtained interferogram and coherence amplitude images are shown in Figures 5 and 6, respectively; here, P–band is selected as an example.

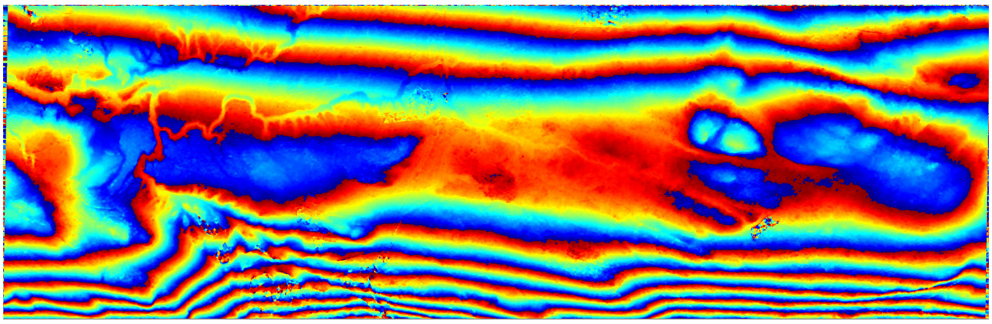

Figure 5. P–band interferometric phase in the study area.

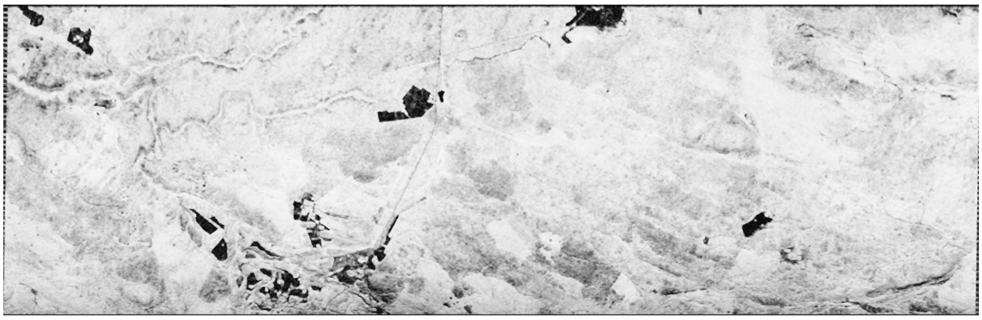

Figure 6. P–band interferometric coherence amplitude imagen the study area.

3.3. Forest Height Estimation Accuracy Evaluation Method

In order to evaluate the accuracy of the inversed forest height, the accuracy evaluation indices selected in this paper included the coefficient of determination (R^2), the Root Mean Square Error (RMSE), and the estimation Accuracy (Acc.). For the details of the calculation of R^2, RMSE, and Acc, readers are referred to [41].

4. Results and Discussion

4.1. Simulated Data

4.1.1. Forest Height Inversion Using RVoG Model and Simulated Data

The results are shown in Figure 7. From the sub-figures, we can see that the shapes of the obtained forest height inversion maps at the L– and P–bands are similar to the simulated forest SAR images. However, the missing values in the mapped forest height inversed results using the X– and C–bands are obvious. It may result from weak penetration capability and obvious shadows on the forest edges [37,38]. At the X–band, the inversion results do not vary significantly with the growth of the baseline—it may result from the lower height of ambiguity (HOA) of the set baseline length at the X–band. For the C–band, the missing forest height results are more obvious at 10 × 2 m and 10 × 4 m, while the missing forest height results are relatively less when the baseline grows to 10 × 6 m and 10 × 8 m.

The pre-set forest height for the simulated data is 18 m, as shown in Figure 7. We found the estimated forest height values, especially inversed using the L– and P–bands using different baseline sets, fluctuate around 18 m. It seems that the forest height inversion results are affected not only by the selection of the wavelength but also by the baseline length. Since the limitation of HOA values of the set baseline length at the X–band, the inversion results do not vary significantly with the baseline, and only a small number of results are equal to the true value under various baseline lengths. At C–band, the forest height is seriously underestimated, especially using the baseline combinations of 10 × 2 m and 10 × 4 m. The estimated forest height results show better performance at the C–band when the baseline combinations are 10 × 6 m and 10 × 8 m. Even in some places, the forest height is seriously underestimated, but the estimated height in most of the other areas fluctuates around the true value. The inversion forest height using the

L–band performed better than the C–band, although there is a certain overestimation of forest height when using the baseline combinations of 10 × 2 m and 10 × 4 m. But with the baseline increasing, the inversion results of forest height are closer to the true value, and most of the estimated values range between 15 m and 20 m. The estimated forest height using the P–band PolInSAR datasets performed well at four baseline combinations. The results show obvious overestimation at each baseline combination, but with the baseline combination of 10 × 8 m, more of the estimated values are 15~20 m, and only a few values are in the range of 25~35 m. In general, at the baseline datasets set in this study, the L– and P–bands show better performance than the C– and X–bands; the longer the baseline length, the better the inversed forest height. Ref. [29] analyzed the relationship between k_z, forest height, and extinction values and summarized the best k_z values for different forest height range estimations at a fixed extinction value. The study did not consider the band used in inversion directly. Compared with this study, the k_z values used in our studies at different bands are a bit different: for the X– and C–bands, the extinction coefficient is set as 0.1 dB/m, for the L–band, it is 0.2 dB/m, and it is 0.4 dB/m for P–band. However, several k_z values which were revealed as having better performance in forest height were partly confirmed in our study. The better performance of the L– and P–bands using RvoG models for forest height inversion were demonstrated in [33,37].

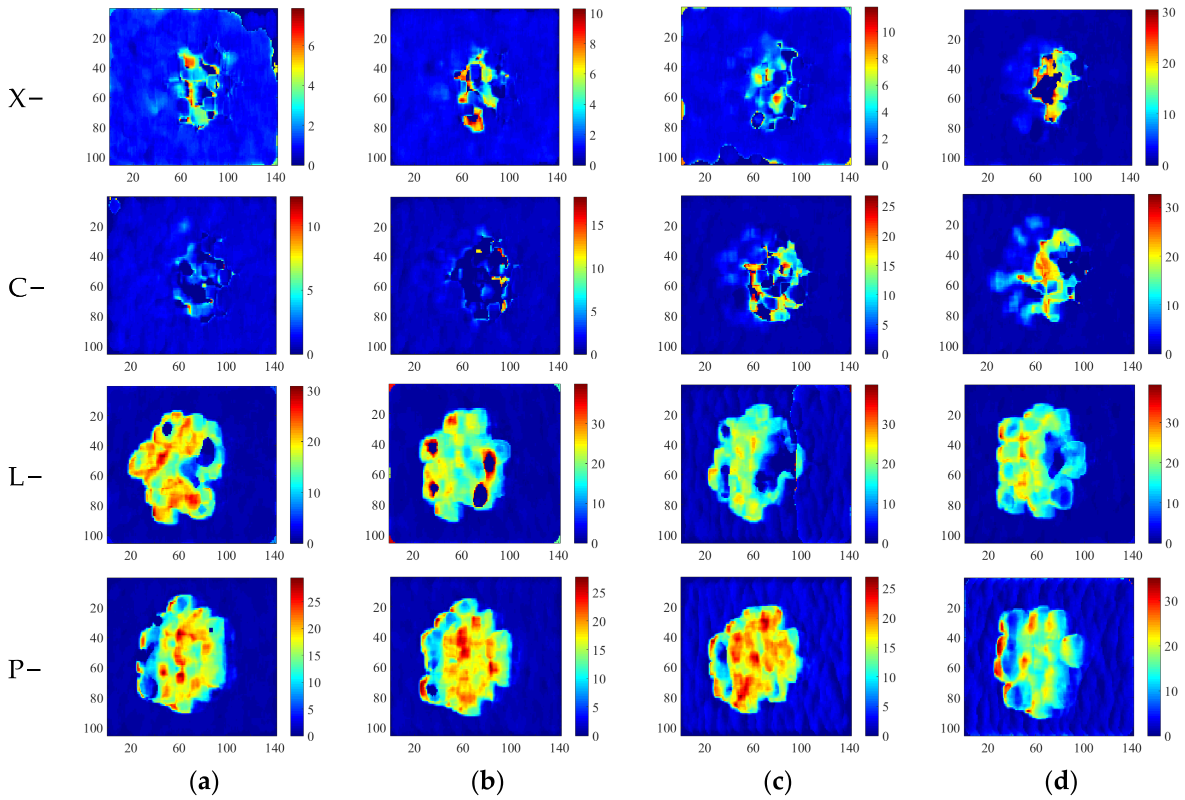

Figure 7. Forest height inversion results. (**a**) 10 × 2 m; (**b**) 10 × 4 m; (**c**) 10 × 6 m; (**d**) 10 × 8 m.

4.1.2. Uncertainty Analysis of Estimation Results

In order to analyze the distribution characteristics of the inversed results, Cumulative Distribution Function (CDF) plots were generated, as shown in Figure 8. Each plot is drawn from 50 randomly selected points in the forest area from the inversed results using the above-mentioned four bands with different baseline combinations. In Figure 9, the simulated data generated for these experiments set the mean forest height as 18 m, and the related values are shown as black dash lines in the sub-figures. It can be seen that the results in the long wavelength, like the L– and P–bands, are accumulated at 18 m, while the estimated results using short wavelengths, like the X– and C–bands, have peaks between 0 m and 5 m, which revealed the obvious underestimation of forest height using the X– and

C–bands PolInSAR datasets. At the X–band, only the results using a baseline combination of 10 × 8 m show a wider dynamic range of estimated results, while for the C–band, both of the baseline combinations of 10 × 6 m and 10 × 8 m have a wide dynamic range of the estimated values. In the L–band, the distributions of the estimated values in various baseline combinations are similar, with two peaks between 0–5 m and 15–25 m, and most of the values fluctuated around 18 m, but the distribution of the results is more discrete, and the dynamic range is larger when compared with the performance of P–band. In the P–band, the results of each baseline combination show a highly aggregated distribution near the true value, especially the baseline combination of 10 × 4 m. The 10 × 4 m baseline combination achieved the best performance in this study, with the highest frequency distribution close to the true value.

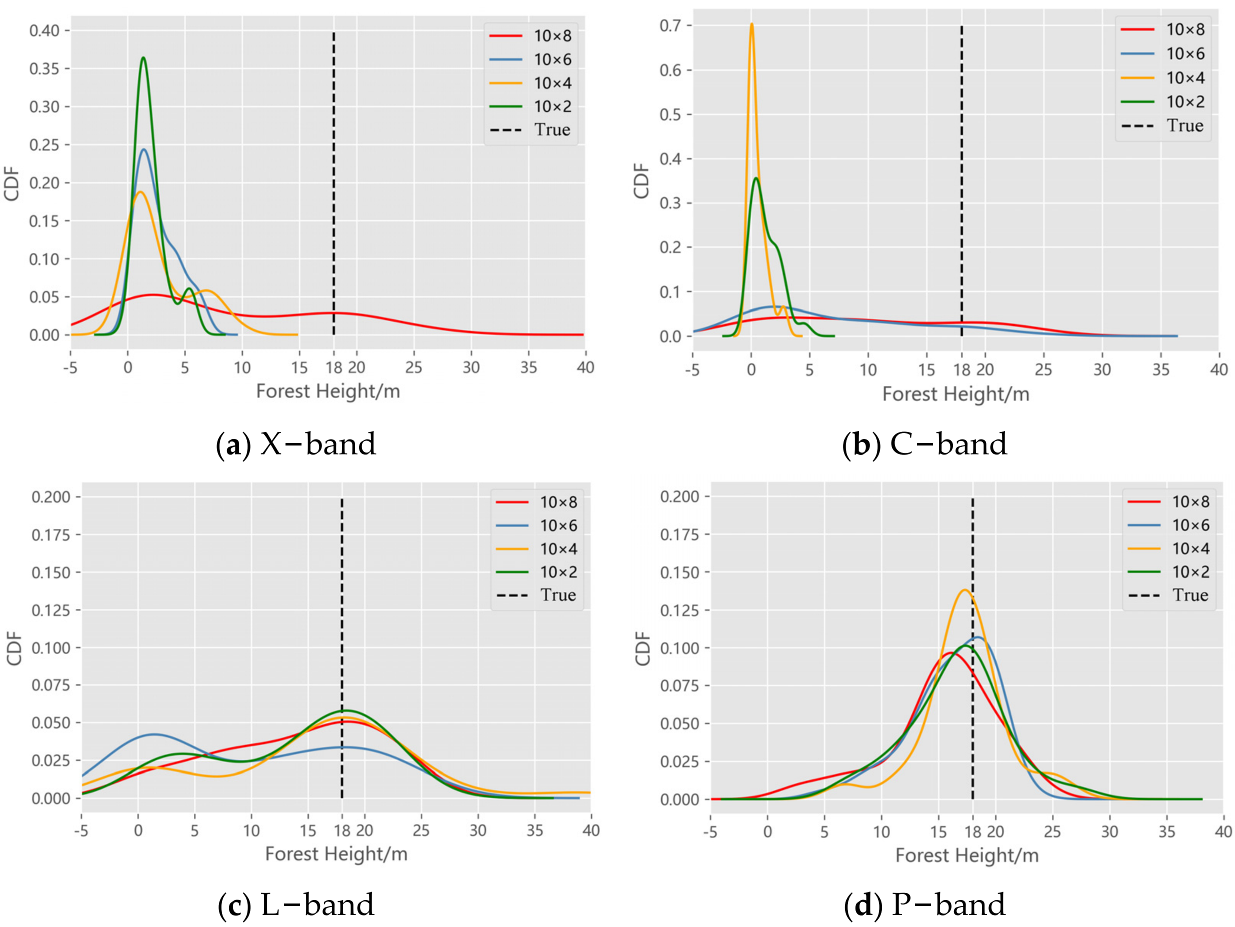

Figure 8. CDF of the inversed forest height using X–, C–, L–, and P–band PolInSAR datasets with different baseline combinations.

The mean and standard deviation (sd) statistics of the inversed results are summarized in Table 3. For the X–band, when the baseline is less than 10 × 8 m, most of the estimated forest height is around 2 m and 3 m, and the sd values range from 1 m to 3 m, while the results obtained by the baseline combination of 10 × 8 m showed better accuracy with mean value of 8.94 m, nonetheless, its sd value is 8.26 m which indicated that the dispersion of the estimated results and poor forest height estimation using the X–band data. In the C–band, the mean and sd values of the inversion results using baseline combinations of 10 × 2 m and 10 × 4 m are less than 2 m, while when the baseline combination increases to 10 × 6 m, the mean value reaches 7.09 m and the sd reaches 6.85 m, and when the baseline combination reaches 10 × 8 m, the mean value of the results reaches 10.1 m and the sd is 7.92 m. The results acquired using the C–band PolInSAR data revealed better performance of the longer baseline. In the L–band, the best inversion results are also obtained when the baseline is 10 × 8 m with a mean value of 13.83 m and sd of 7.14 m. The best performance of the P–band was obtained with a baseline combination of 10 × 4 m with mean = 17.22 m and sd = 3.63 m. The results acquired at short wavelength resulted in longer baseline combinations that may improve the estimation results. However, with the penetration limitation of the X– or C–bands, the inversion uncertainties were improved. Coherence analysis of the X–band TanDEM InSAR datasets in [42] also demonstrated that greater uncertainties resulted from low coherence values using longer baseline combinations.

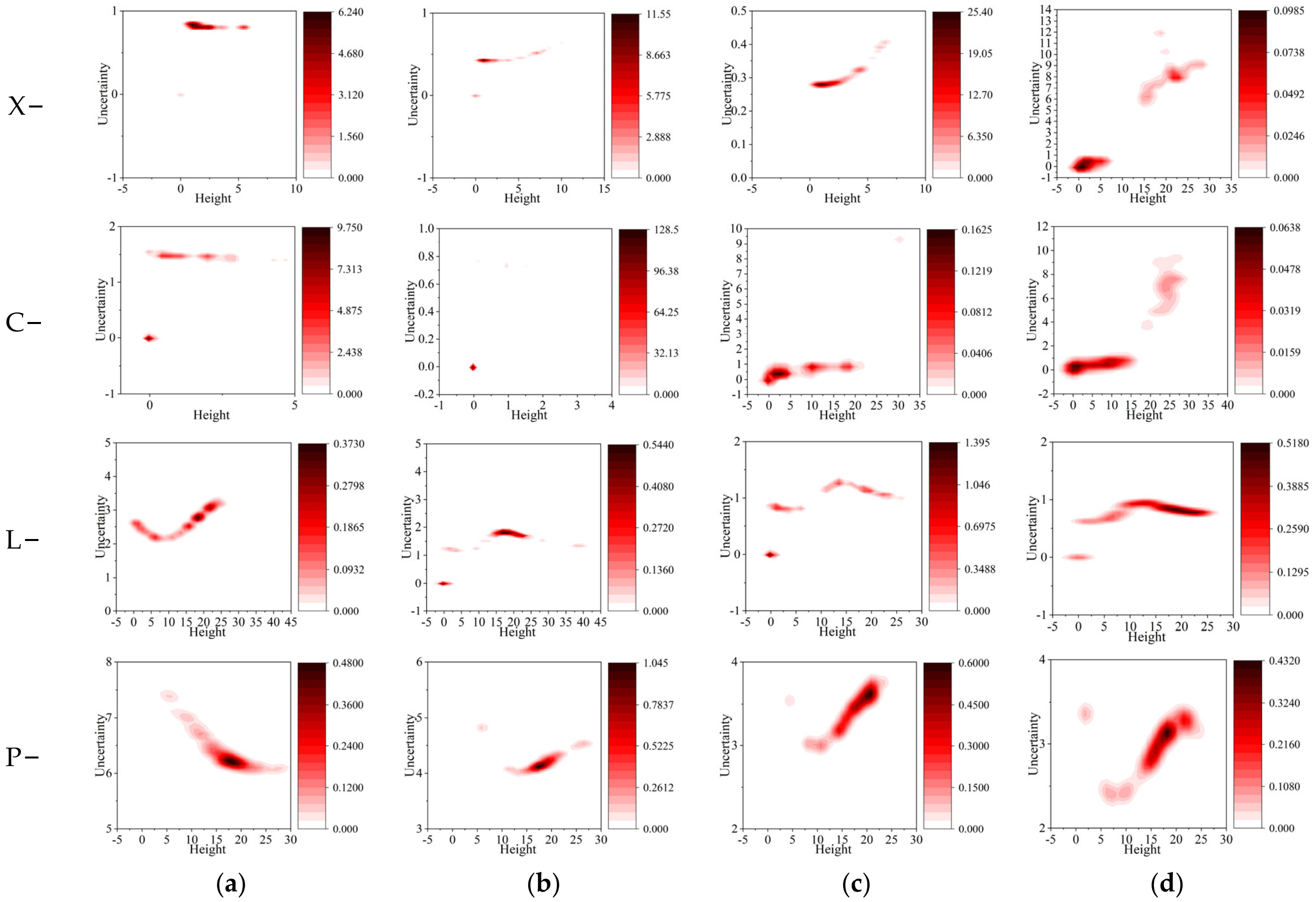

Figure 9. Two–dimensional histogram between uncertainties of estimated forest height and the forest height estimated using RVoG models. (**a**) 10 × 2 m; (**b**) 10 × 4 m; (**c**) 10 × 6 m; (**d**) 10 × 8 m.

Table 3. Sample forest height inversion results (unit: m).

Band	X–		C–		L–		P–	
Baseline	**Mean**	**sd**	**Mean**	**sd**	**Mean**	**sd**	**Mean**	**sd**
10 × 2	2.03	1.37	1.23	1.17	13.78	7.22	16.54	4.25
10 × 4	2.82	2.73	0.53	0.77	15.31	9.24	17.22	3.63
10 × 6	2.59	1.74	7.09	6.85	10.22	8.77	16.21	3.67
10 × 8	8.94	8.26	10.1	7.92	13.83	7.14	15.38	4.67

4.1.3. Bayesian-Based Uncertainty Analysis and Decrease

To further analyze the uncertainty of the forest height inversed results, a Bayesian probabilistic framework is used to simultaneously obtain the sampling points according to the posterior distribution of forest height and its uncertainty based on the inversion of simulated PolInSAR data. Firstly, the mean value of the estimated forest height using the RvoG model works as the mean of the prior Gaussian distribution, and the standard deviation for Gaussian distribution is set as 10 m, with the fixed extinction coefficients for each band, the posterior distributions were generated based on a developed hierarchical Bayesian framework. Then, the new estimated forest height series were generated by the sampling according to the posterior distributions of the hierarchical Bayesian frameworks. The readers are referred to [26,37] for detailed procedures for posterior distribution calculation and sampling. The uncertainties calculated with Bayesian algorithms and their relationships with forest height were plotted as shown in Figure 9, where the horizontal axis is the forest height and the vertical axis is the uncertainty (i.e., the average sd of the posterior sampled forest height. For short wavelength bands like the X–band and the C–band, when the baseline length is 10×2 m and 10×4 m, the uncertainties do not change significantly with height, but when the baseline grows, the uncertainty starts to increase with height. For long wavelength bands like the L– and P–bands, when the baseline length is 10×2 m and 10×4 m, the uncertainty tends to decrease with increasing height, with the forest height ranging from 0 m to 10 m, and it tends to increase with increasing height when the forest height continues to increase. Note that at L–band, when the baseline combinations are larger than 10×4 m, the accumulations of uncertainty values showed an obvious decrease with the increase in baseline length, and their relationships with forest height are not clear. However, for the P–band, the uncertainties showed increased trends with the increasing forest height. The peak uncertainty values increased with the increase in baseline length.

Table 4 summarizes the forest height results sampled by Bayesian posterior distribution functions and Metropolis–Hastings Algorithms for different combinations of baseline at each band. In the X– and C–bands, although the mean absolute error decreases with the growth of the baseline and the prediction accuracy increases with the growth of the baseline, the best estimation results appear at a baseline of 10×8 m, but combined with Figure 9, it seems that the uncertainty also increases with the growth of the baseline. For the L– and P–bands, the best results were obtained at a baseline of 10×4 m, and the results became worse when the baseline continued to grow. This phenomenon indicated that the applicable baseline lengths are different for different bands, and the appropriate baseline lengths should be chosen for different bands to obtain reliable inversion results. Moreover, the uncertainties of estimated forest height obviously reduced when we compared the uncertainties and forest height results acquired from the posterior distribution function (Table 4) with the original estimated forest height using the RVoG model (Table 3). The results revealed the capability of the Bayesian framework to reduce the estimation uncertainties [26].

Table 4. Bayesian posterior sampling results.

Band	Baseline	True Forest Height (m)	Mean + sd (m) from Bayesian	δ (m)	Acc.
X–	10×2	18	2.03 ± 0.80	15.97	0.11
	10×4		2.83 ± 0.41	15.17	0.16
	10×6		2.6 ± 0.30	15.4	0.14
	10×8		10.56 ± 3.80	7.44	0.59
C–	10×2	18	1.17 ± 1.14	16.83	0.07
	10×4		0.52 ± 0.35	17.48	0.03
	10×6		7.24 ± 0.72	10.76	0.40
	10×8		11.15 ± 2.33	6.85	0.62
L–	10×2	18	14.18 ± 2.67	3.82	0.79
	10×4		15.37 ± 1.44	2.63	0.85
	10×6		10.2 ± 0.85	7.8	0.57
	10×8		13.82 ± 0.76	4.18	0.77
P–	10×2	18	16.56 ± 6.38	1.44	0.92
	10×4		17.5 ± 4.21	0.05	0.97
	10×6		17.08 ± 3.42	0.92	0.95
	10×8		16.15 ± 2.99	0.75	0.90

4.2. Airborne PolInSAR Data

According to the forest height estimated above using the simulated data, the L– and P–bands performed better for forest height estimation. To investigate the uncertainty resulting from baseline length on the forest height inversion results in real forest scenarios, the L– and P–bands airborne PolInSAR datasets with three different baselines were applied to forest height inversion using the RVoG model. The estimated results and their uncertainties analysis and decrease are summarized in this section. Based on the optimal complex coherence obtained in Section 3.2.3, the forest height is obtained by the RVoG model. Figure 10 shows the results of geocoded forest height inversion results, the results acquired with an 18 m spatial baseline at the L–band and the results acquired with a 24 m spatial baseline at the P–band were selected here as examples. A total of 41 forest stands were surveyed during the BioSAR2008 activity. To avoid selecting non–forest areas for quantitative evaluation of forest height in the RVoG model, 150 sample points were randomly selected within the 41 stands, and LiDAR data were used as reference values to evaluate the accuracy of the estimated forest height results. The spatial distribution of forest stands and sample points for validation is shown in Figure 10c.

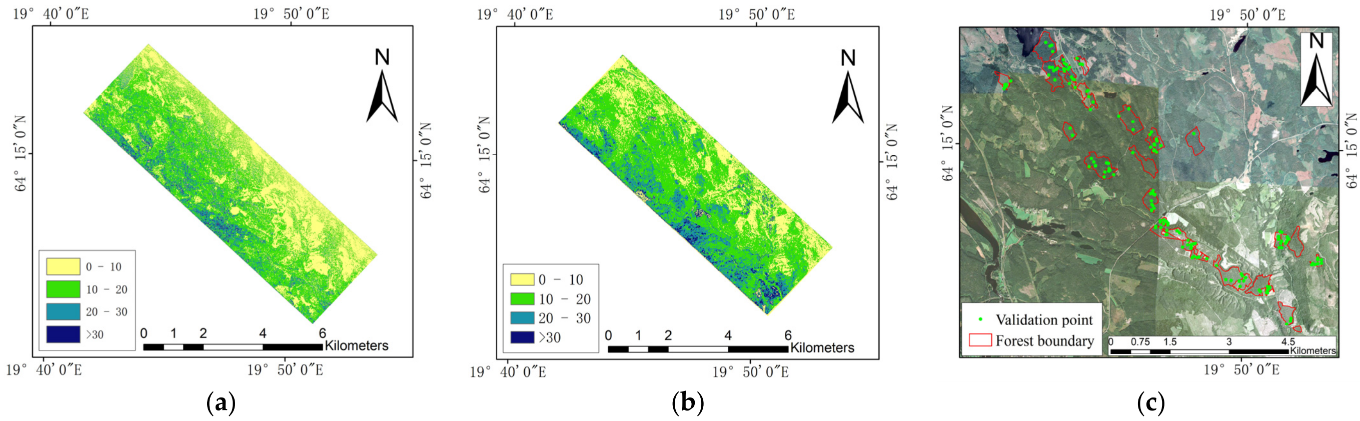

Figure 10. The inversed forest height using RVoG models and L–and P–band PolInSAR datasets. (**a**) L–band (18 m spatial baseline); (**b**) P–band (24 m spatial baseline); (**c**) Spatial distribution of selected forest stands and validation plots.

4.2.1. Forest Height Inversion Using RVoG Model and Airborne PolInSAR Datasets

In this paper, a total of six spatial baseline combinations at L– and P–bands were used for forest height inversion using the RVoG model. The accuracies of the inversed results of each baseline combination are shown in Figure 11. Figure 11 shows the scatter plots between the inversed forest height values against LiDAR CHM values. In Figure 11, (a), (c), and (e) are for height-estimated results of the L–band with different baseline combinations; In Figure 11, (b), (d), and (f) are the acquired results for the P–band.

For the performance of the L–band PolInSAR datasets, the results acquired using a 6 m spatial baseline of the L–band showed the worst performance in the three selected baselines. The estimated results showed large dispersion with R^2 = 0.11, RMSE = 9.49 m, and Acc. = 34.38%. When the baseline increases to 12 m in Figure 12c, the inversed results obviously improve with R^2 of 0.42, RMSE of 4.86 m, and Acc. of 67.50%. When the spatial baseline increases to 18 m, the R^2 reaches a maximum of 0.64, the RMSE reaches a minimum of 3.32 m, and the Acc. has the highest value of 77.78%. The results acquired at the L–band revealed that with the increase in baseline, the accuracy of inversion is increased. Meanwhile, the distribution of the scatter plots in (e) showed reduced overestimation and underestimation errors when compared with (c), while the overestimation and underestimation errors in (c) are also better than that in (a). The performance of the P–band shows a similar trend to the L–band; the longer baseline dataset performed better than the shorter baseline for the forest height inversion. The best performance was acquired at the baseline of 24 m with R^2 of 0.51, RMSE of 3.82 m, and Acc. of 74.44%. The worst performance was acquired with a baseline of 8 m with R^2 = 0.17, RMSE = 11.95 m, and Acc. = 19.28%. Not that the P–band with a 24 m baseline performed better than the L–band with a 12 m baseline but worse than the L–band with an 18 m baseline. However, both the L– and P–bands showed better performance when the baseline was higher than 8 m. The Acc. values range from 65% to 80%. The results also revealed the estimated accuracy depends on the wavelength and baselines. It is crucial to choose a suitable spatial baseline when using the RVoG model for forest height estimation. This also agrees with [27,37,38].

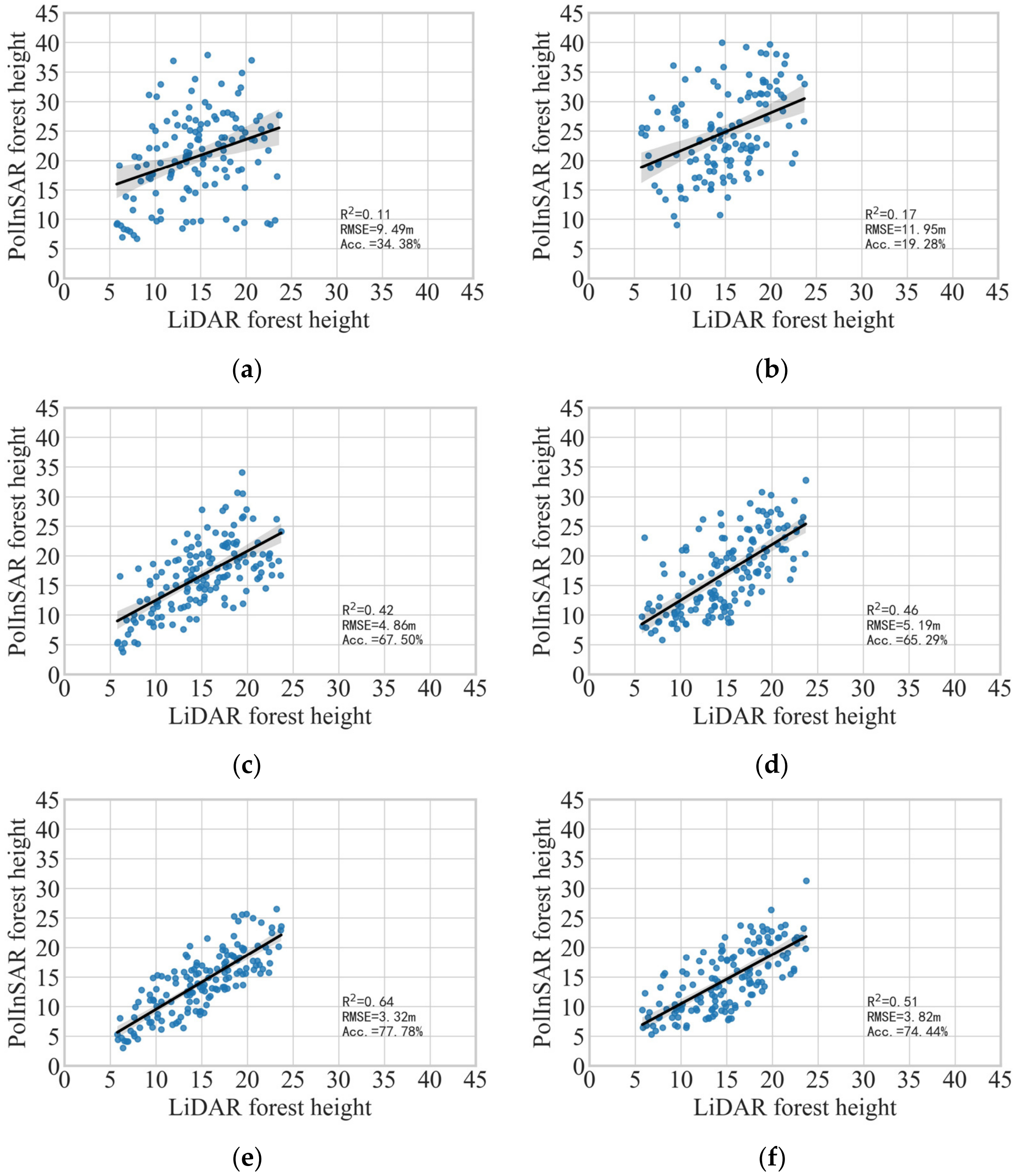

Figure 11. Scatterplot of estimated accuracy. (**a**) L–band (6 m spatial baseline); (**b**) P–band (8 m spatial baseline); (**c**) L–band (12 m spatial baseline); (**d**) P–band (16 m spatial baseline); (**e**) L–band (18 m spatial baseline); (**f**) P–band (24 m spatial baseline).

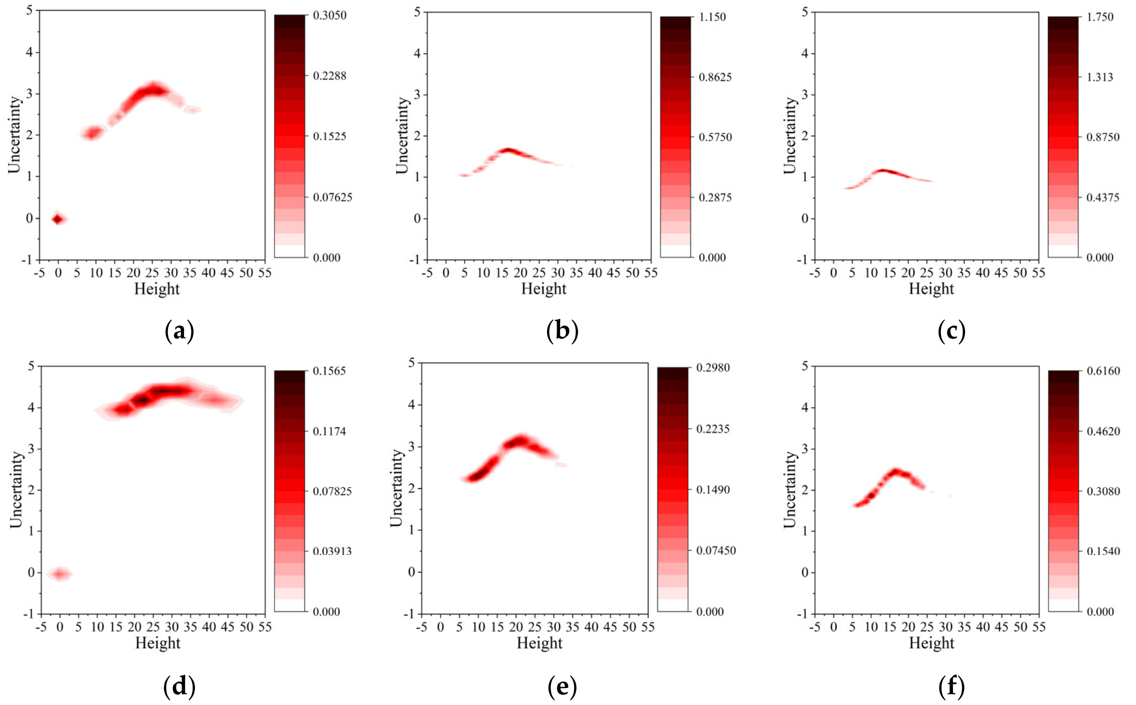

Figure 12. Standard deviation of RVoG height and two–dimensional histogram of RVoG height. (**a**) L–band (6 m spatial baseline); (**b**) L–band (12 m spatial baseline); (**c**) L–band (18 m spatial baseline); (**d**) P–band (8 m spatial baseline); (**e**) P–band (16 m spatial baseline); (**f**) P–band (24 m spatial baseline).

4.2.2. Bayesian-Based Uncertainty Analysis of Estimation Results

The estimation uncertainties calculated by Bayesian algorithms and their relationships with forest height were plotted, as shown in Figure 12. The accumulated uncertainties of the estimated results—both using the L– and P–bands—decreased with the increasing baseline length. Different from the results of simulated datasets, the uncertainties both at the L– and P–bands first showed an increasing trend and then a decreasing trend with the change in forest height. The turning points for the L–band are around 25 m, 18 m, and 13 m for 6 m, 12 m, and 18 m baselines, respectively. While for the P–band, the turning points are approximately 30 m, 22 m and 18 m, respectively. According to the k_z values of simulated PolInSAR datasets and the airborne datasets, the trend of uncertainties was similar for each band. For example, at the P–band, the uncertainties increase, with k_z ranging from 0.02 dB/m to 0.05 dB/m and height less than 18 m.

Table 5 shows the posterior sampling results of the airborne data forest height, from which it can be seen that the average absolute error gradually decreases with the growth of the baseline while its prediction accuracy gradually increases. The best results are obtained for the L–band when the baseline length is 18 m and for the P–band when the baseline length is 24 m. With the comparison of the original estimated forest height values, the acquired forest height values from the sampling of the Bayesian posterior distribution function showed lower uncertainties and an obvious increase in accuracy. Here, the results acquired at the L–band were better than those acquired at the P–band. Since the different baseline sets were selected for the L– and P–bands for forest height inversion using RVoG models, it is not easy to demonstrate that the L–band performed better than the P–band. Meanwhile, the P–band simulated datasets performed better than the L–band with a homogeneous forest scene. The results may reveal the obvious effects of forest structure on forest height inversion. This may result from the capability of RVoG to describe the forest structures. However, the results confirmed the good performance of the L– and P–bands for forest height inversion using the RVoG model with a suitable baseline length.

Table 5. Posterior distribution sampling results for L-band and P-band.

Band	Baseline	Mean Forest Height	Mean ± sd (m) from Bayesian	δ (m)	Acc.
L–	6 m	20.60 m	18.65 ± 2.43	3.7	0.75
	12 m	16.59 m	16.64 ± 1.48	1.69	0.89
	18 m	14.06 m	14.08 ± 1.03	0.87	0.94
P–	8 m	26.40 m	26.14 ± 4.03	11.19	0.25
	16 m	17.11 m	17.77 ± 2.76	2.82	0.81
	24 m	14.56 m	14.02 ± 2.12	0.93	0.94

5. Conclusions

With the forest height estimation using simulated PolInSAR datasets with four different baselines at each band and the similar procedure of using L– and P–band airborne PolInSAR datasets with three different baseline lengths, we explored the influence of wavelength and baseline length on forest height inversion and the potential of using Bayesian framework for uncertainty quantification and decrease. It concluded that: (1) wavelength affected the inversion results of forest height using RVoG models. Longer wavelengths like the L– and P–bands performed better in forest height inversion. (2) It is crucial to select a suitable baseline length to obtain the best forest height inversion results. In this study, the longer baseline showed better performance in forest height inversion. However, due to the relationship between k_z and baseline length, it is not the case that the longer the baseline, the better the results for estimating forest height. The suitable baselines need to be selected according to forest height, forest structure, and other factors which need to be further explored in the future. (3) Successful application of the RVoG model requires certain assumptions about the imaged forest and acquisition scenario to reduce the error in forest height estimation. The quantification of the error and uncertainty in height estimation is limited to external validation data, and the Bayesian framework takes into account the error caused by RVoG modeling, making the framework useful for quantifying the uncertainty in the estimation of forest height. It has the ability to reduce the estimation uncertainty by using the posterior distribution function and to perform sampling to reduce estimation uncertainty. Since only several baselines were selected in this study, the influence of other baseline lengths on forest height inversion using PolInSAR datasets and RVoG models needs to be further explored for setting the most suitable baseline length for forest height inversion.

Author Contributions: Conceptualization, W.Z.; methodology, Y.Z.; project administration, W.Z.; resources, W.Z.; software, Y.Z., H.Z. and Y.J.; supervision, W.Z. and Y.J.; validation, Y.Z., T.Z. and Y.J.; writing—original draft preparation, Y.Z. and W.Z.; writing—review and editing, Y.Z., W.Z. and H.Z.; visualization, Y.Z. and H.Z. All authors have read and agreed to the published version of the manuscript.

Funding: This research was funded by the National Natural Science Foundation of China (grant numbers:32160365, 42161059, and 31860240) and by the Agriculture joint special project of Yunnan province (grant number: 202301BD070001−058).

Data Availability Statement: Not applicable.

Acknowledgments: The authors would like to thank Tingwei Zhang for her contribution to the preliminary work of this paper.

Conflicts of Interest: The authors declare no conflict of interest.

References

1. Houghton, R.A.; Hall, F.; Goetz, S.J. Importance of Biomass in the Global Carbon Cycle: Biomass in the global carbon cycle. *J. Geophys. Res.* **2009**, *114*, G00E03. [CrossRef]
2. Liu, X.; He, L.; He, Z.; Wei, Y. Estimation of Broadleaf Tree Canopy Height of Wolong Nature Reserve Based on InSAR and Machine Learning Methods. *Forests* **2022**, *13*, 1282. [CrossRef]

3. Zhao, R.; Cao, S.; Zhu, J.; Fu, L.; Xie, Y.; Zhang, T.; Fu, H. A Dual–Baseline PolInSAR Method for Forest Height and V ertical Profile Function Inversion Based on the Polarization Coherence Tomography Technique. *Forests* **2023**, *14*, 626. [CrossRef]
4. Wang, L.; Zhou, Y.; Shen, G.; Xiong, J.; Shi, H. Forest Height Inversion Based on Time–Frequency RVoG Model Using Single–Baseline L–Band Sublook–InSAR Data. *Remote. Sens.* **2023**, *15*, 166. [CrossRef]
5. Khati, U.; Singh, G.; Kumar, S. Potential of Space–Borne PolInSAR for Forest Canopy Height Estimation Over India—A Case Study Using Fully Polarimetric *L* –, *C* –, and *X* –Band SAR Data. *IEEE J. Sel. Top. Appl. Earth Obs. Remote. Sens.* **2018**, *11*, 2406–2416. [CrossRef]
6. Fan, Y.X. *Forest Height Estimation Method Using Space–Borne X–B and SAR Interferometry*; Chinese Academy of Forestry: Beijing, China, 2019.
7. Balzter, H.; Luckman, A.; Skinner, L.; Rowland, C.; Dawson, T. Observations of Forest Stand Top Height and Mean Height from Interferometric SAR and LiDAR over a Conifer Plantation at Thetford Forest, UK. *Int. J. Remote Sens.* **2007**, *28*, 1173–1197. [CrossRef]
8. Kaasalainen, S.; Holopainen, M.; Karjalainen, M.; Vastaranta, M.; Kankare, V.; Karila, K.; Osmanoglu, B. Combining Lidar and Synthetic Aperture Radar Data to Estimate Forest Biomass: Status and Prospects. *Forests* **2015**, *6*, 252–270. [CrossRef]
9. Luo, H.M. *Models and Methods of Extracting Froest Structure Information by Polarimetric SAR Interferometry*; University of Electronic Science and Technology of China: Beijing, China, 2011.
10. Feng, Q. *Land Cover Types Classification by Support Vector Machines Using Multi–Temporal Polarimetric SAR Data*; Chinese Academy of Forestry: Beijing, China, 2012.
11. Niu, C.Y.; Ma, D.B.; Zhang, X.F. Study on PolSAR Classification Based on H/α/A Decomposition for Crops. *J. Inf. Eng. Univ.* **2006**, *7*, 404–407.
12. Ling, F.L.; Li, Z.Y.; Chen, E.X.; Huang, Y.P.; Tian, X. Regional Forest and Non–Forest Mapping Using Envisat ASAR Data. *J. Remote Sens.* **2012**, *16*, 1100–1113.
13. Li, L. *Forest Vertical Information Extraction Based on P–Band SAR Tomography*; Chinese Academy of Forestry: Beijing, China, 2016.
14. Guo, H.D.; Li, X.W.; Wang, C.L.; Li, Z. The Mechanism and Role of Polarimetric SAR Interferometry. *J. Remote Sens.* **2002**, *6*, 401–405.
15. Li, X.W.; Guo, H.D.; Liao, J.J.; Wang, C.L.; Yan, F.L. Inversion of Vegetation Parameters Using Spaceborne Polarimetric SAR Interferometry. *J. Remote Sens.* **2002**, *6*, 424–429.
16. Sa, R.; Nei, Y.; Fan, W. Combining Multi–Dimensional SAR Parameters to Improve RVoG Model for Coniferous Forest Height Inversion Using ALOS–2 Data. *Remote. Sens.* **2023**, *15*, 1272. [CrossRef]
17. Cloude, S.R.; Papathanassiou, K.P. Three–Stage Inversion Process for Polarimetric SAR Interferometry. *IEE Proc. –Radar Sonar Navig.* **2003**, *150*, 125–134. [CrossRef]
18. Cloude, S.R.; Papathanassiou, K.P. Polarimetric SAR Interferometry. *IEEE Trans. Geosci. Remote Sens.* **1998**, *36*, 1551–1565. [CrossRef]
19. Treuhaft, R.N.; Madsen, S.N.; Moghaddam, M.; van Zyl, J.J. Vegetation Characteristics and Underlying Topography from Interferometric Radar. *Radio Sci.* **1996**, *31*, 1449–1485. [CrossRef]
20. Treuhaft, R.N.; Cloude, S.R. The Structure of Oriented Vegetation from Polarimetric Interferometry. *IEEE Trans. Geosci. Remote Sens.* **1999**, *37*, 2620–2624. [CrossRef]
21. Treuhaft, R.N.; Siqueira, P.R. Vertical Structure of Vegetated Land Surfaces from Interferometric and Polarimetric Radar. *Radio Sci.* **2000**, *35*, 141–177. [CrossRef]
22. Managhebi, T.; Maghsoudi, Y.; Amani, M. Forest Height Retrieval Based on the Dual PolInSAR Images. *Remote Sens.* **2022**, *14*, 4503. [CrossRef]
23. Dubois-Fernandez, P.C.; Souyris, J.-C.; Angelliaume, S.; Garestier, F. The Compact Polarimetry Alternative for Spaceborne SAR at Low Frequency. *IEEE Trans. Geosci. Remote Sens.* **2008**, *46*, 3208–3222. [CrossRef]
24. Garestier, F.; Dubois-Fernandez, P.C.; Champion, I. Forest Height Inversion Using High–Resolution P–Band Pol–InSAR Data. *IEEE Trans. Geosci. Remote Sens.* **2008**, *46*, 3544–3559. [CrossRef]
25. Zhu, J.J.; Xie, Q.H.; Zuo, T.Y.; Wang, C.C.; Xie, J. Criterion of Complex Least Squares Adjustment and Its Application in Tree Height Inversion with PolInSAR Data. *Acta Geod. Et Cartogr. Sin.* **2014**, *43*, 45–51. [CrossRef]
26. Riel, B.; Denbina, M.; Lavalle, M. Uncertainties in Forest Canopy Height Estimation from Polarimetric Interferometric SAR Data. *IEEE J. Sel. Top. Appl. Earth Obs. Remote. Sens.* **2018**, *11*, 3478–3491. [CrossRef]
27. Kugler, F.; Lee, S.-K.; Hajnsek, I.; Papathanassiou, K.P. Forest Height Estimation by Means of Pol–InSAR Data Inversion: The Role of the Vertical Wavenumber. *IEEE Trans. Geosci. Remote Sens.* **2015**, *53*, 5294–5311. [CrossRef]
28. Liao, Z.M. *Forest Aboveground Biomass Estimation Using PolInSAR Data*; University of Electronic Science and Technology of China: Chengdu, China, 2019.
29. Askne, J.I.H.; Dammert, P.B.G.; Ulander, L.M.H.; Smith, G. C–Band Repeat–Pass Interferometric SAR Observations of the Forest. *IEEE Trans. Geosci. Remote Sens.* **1997**, *35*, 25–35. [CrossRef]
30. Askne, J.I.H.; Soja, M.J.; Ulander, L.M.H. Biomass Estimation in a Boreal Forest from TanDEM–X Data, Lidar DTM, and the Interferometric Water Cloud Model. *Remote Sens. Environ.* **2017**, *196*, 265–278. [CrossRef]
31. Soja, M.J.; Persson, H.; Ulander, L.M.H. Estimation of Forest Height and Canopy Density from a Single InSAR Correlation Coefficient. *IEEE Geosci. Remote Sens. Lett.* **2015**, *12*, 646–650. [CrossRef]

32. Managhebi, T.; Maghsoudi, Y.; Valadan Zoej, M.J. An Improved Three–Stage Inversion Algorithm in Forest Height Estimation Using Single–Baseline Polarimetric SAR Interferometry Data. *IEEE Geosci. Remote Sens. Lett.* **2018**, *15*, 887–891. [CrossRef]
33. Zhang, W.F.; Chen, E.X.; Li, Z.Y.; Zhao, L.; Ji, Y.J. Development of Forest Height Estimation Using InSAR/PolInSAR Technology. *Remote Sens. Technol. Appl.* **2017**, *32*, 983–997.
34. Wu, W.; Clark, J.S.; Vose, J.M. Assimilating Multi–Source Uncertainties of a Parsimonious Conceptual Hydrological Model Using Hierarchical Bayesian Modeling. *J. Hydrol.* **2010**, *394*, 436–446. [CrossRef]
35. Gelfand, A.E.; Hills, S.E.; Racine-Poon, A.; Smith, A.F.M. Illustration of Bayesian Inference in Normal Data Models Using Gibbs Sampling. *J. Am. Stat. Assoc.* **1990**, *85*, 972–985. [CrossRef]
36. Gelfand, A.E.; Smith, A.F.M. Sampling–Based Approaches to Calculating Marginal Densities. *J. Am. Stat. Assoc.* **1990**, *85*, 398–409. [CrossRef]
37. Zhang, T.W. *Uncertainty Analysis in Forest Height Inversion Using Polarimetric SAR Interferometric Data*; Southwest Forestry University: KunMing, China, 2021.
38. Zhang, T.W.; Zhang, W.F.; Zhang, Y.X.; Huang, G.R. Bayesian Analysis for Uncertainty of Forest Height Inversed by Polarimetric Interferometric SAR Data. *Natl. Remote Sens. Bull.* **2021**, 1–15. [CrossRef]
39. Williams, M.L.; Pottier, E.; Ferro-Famil, L.; Allain, S.; Cloude, S.R.; Consultants, A.; Hajnsek, I.; Papathanassiou, K.; Moreira, A.; Minchella, A.; et al. Forest coherent sar simulation within polsarpro: An educational toolbox for polsar and polinsar data processing. *Asian Conf. Remote Sens.* **2007**.
40. Neumann, M.; Saatchi, S.S.; Ulander, L.M.H.; Fransson, J.E.S. Assessing Performance of L– and P–Band Polarimetric Interferometric SAR Data in Estimating Boreal Forest Above–Ground Biomass. *IEEE Trans. Geosci. Remote Sens.* **2012**, *50*, 714–726. [CrossRef]
41. Fan, Y.; Chen, E.; Li, Z.; Zhao, L.; Zhang, W.; Jin, Y.; Cai, L. Forest Height Estimation Method Using TanDEM–X Interferometric Coherence Data. *Sci. Silvae Sin.* **2020**, *56*, 35–46. [CrossRef]
42. Martone, M.; Braeutigam, B.; Rizzoli, P.; Gonzalez, C.; Bachmann, M.; Krieger, G. Coherence evaluation of tandem–x interferometric data. *Isprs J. Photogramm. Remote Sens.* **2012**, *73*, 21–29. [CrossRef]